Collective dynamics of liquid sulfur scrutinized over three decades in frequency

F. Demmel and M. Jimenez-Ruiz

Published version information

Citation: F Demmel and M Jimenez-Ruiz. Collective dynamics of liquid sulfur scrutinized over three decades in frequency. Phys Rev E 106, no. 1 (2022): 014606. doi:10.1103/PhysRevE.106.014606.

DOI: 10.1103/PhysRevE.106.014606

Collective dynamics of liquid sulfur scrutinized over three decades in frequency

F. Demmel[1,*] and M. Jimenez-Ruiz[2]
[1]*ISIS Facility, Rutherford Appleton Laboratory, Didcot OX11 0QX, United Kingdom*
[2]*ILL, 71 Avenue des Martyrs, 38042 Grenoble Cedex 9, France*

(Received 2 February 2022; accepted 6 July 2022; published 21 July 2022)

Liquid sulfur consists mainly of eight-membered rings and hence can be regarded as a model of a molecular liquid. A liquid, which is built from different molecular structures, will demonstrate a wide range in relaxation processes and excitation modes. Three inelastic neutron scattering experiments have been performed to study the collective dynamics of liquid sulfur over three decades in frequencies. A wide range of wave vectors was studied to reveal the response of density fluctuations over different lengthscales. A viscoelastic model with a two-times memory function was applied to the data. The analysis revealed a slow relaxation mode, an acoustic-type excitation, and a high-frequency mode, which resembles an optic-type excitation. The wave-vector dependence of the slow relaxation mode width exhibits the signs of a de Gennes narrowing around the wave vector where the structure factor has a shoulder. This slow relaxation process could be related to diffusive particle movements. The acoustic-type modes evidence a viscoelastic reaction with a 50% enhancement of the sound velocity. This enhancement of the sound velocity and the spectral line shape is qualitatively similar to spectra of molecular liquids. The two relaxation times of the memory function are separated by about two orders of magnitude and underpin the need for a wide frequency range investigation of this complex liquid. The high-frequency response can be interpreted as optic-type modes in the liquid.

DOI: 10.1103/PhysRevE.106.014606

I. INTRODUCTION

Elemental sulfur is a bright yellow, crystalline solid at room temperature. It is the element with the most known crystalline forms in the solid state [1,2]. The orthorhombic structure at room temperature consists of S_8 rings with a bond length of 2.055 Å [3]. At $T = 368.5$ K, below its melting temperature, the structure changes from α-sulfur to the monoclinic β-form [1]. The melting occurs at $T_m = 392.9$ K [1,2]. It is believed that the S_8 rings survive in the liquid and form a liquid with a dominating fraction of eight-membered sulfur rings. At $T = 432$ K, sulfur has a further phase transition to a state with a huge increase in viscosity [4,5]. From density measurements it was concluded that a similarity with the λ-transition in helium exists and hence this transition was coined the λ-transition [6]. The cause for this transition is supposed to be a transformation of the rings into long polymerlike chains [7–10]. With a further increase of temperature, the viscosity starts to drop until the boiling point of sulfur is reached at $T = 718$ K. This large increase of the viscosity and the underlying structural evolution during the polymerization transition is still under debate; see, for example, Refs. [11–16]. Also the diffusion coefficient [17] mirrors that transition as well as light absorption properties [18] and heat capacity [19]. Including pressure as a variable, the phase diagram of sulfur becomes even richer [20]. Density changes in the phase diagram of sulfur have been related with a potential liquid-liquid phase transition and the existence of a further critical point [21].

In addition to this fundamental interest in the properties of sulfur, it occurs with high abundance and is used on a large scale in industry [22]. For industrial applications, the relevant temperature range of sulfur is the liquid range below the λ-transition, when liquid sulfur has a low viscosity. Sulfur has been relevant in the field of geoscience for several decades [23], and more recently it has attracted attention as an abundant cheap material in the field of energy research for novel batteries [24].

Neutron and x-ray diffraction experiments have been performed to reveal the microscopic structure of the liquid state below and above the λ-transition; see, for example, Refs. [25–28]. The structure factor $S(Q)$ is composed of a main structure factor peak at about $Q \approx 1.7$ Å^{-1} and a shoulder at $Q \approx 1.2$ Å^{-1} [29]. This type of structure is not compatible with a simple hard sphere modeling, and it calls for a more sophisticated liquid structure model. The next-nearest neighbor distance was found to be 2.053 Å [29], identical to the value for the crystalline state. This fact is compatible with the idea that liquid sulfur consists of mainly S_8 rings, similar to the crystalline state. With rising temperature, the main peak decreases and the prepeak shoulder increases around the λ-transition [25]. Through analyzing and modeling the pair correlation functions $g(r)$, it was concluded that the λ-transition is related to a reduction of S_8 rings [26,30] and the polymerized state contains a large fraction of chainlike structures [29]. However, modeling of the measured and then Fourier-transformed structure factor delivered sometimes conflicting interpretations about the atomic structure in liquid

*franz.demmel@stfc.ac.uk

sulfur [31,32]. The liquid sulfur structure may not be describable with stable molecular units [33], which differentiates liquid sulfur from a molecular liquid.

Classical MD-simulations have been performed to reveal the structure and dynamics of liquid sulfur [34]. The picture with S_8 rings in the liquid state, which then eventually break up with rising temperature, was confirmed. *Ab initio* molecular dynamics calculations were also applied, and it was concluded that the main elements of the liquid structure are S_8 rings [35], which are then transformed into a mixture of long and short chains at high temperature [36].

To shed light on the question of how the molecular constituents in liquid sulfur can affect thermodynamic and transport quantities, such as the specific heat and viscosity, an investigation is needed of the collective dynamics on molecular lengthscales. In particular, the collective dynamics can provide valuable information about the interrelation of structure and dynamics due to their connection between wave vector and excitation frequency, coined the dispersion relation. In recent years, the collective dynamics of many liquids, in particular so-called simple ones, have been investigated. One common feature was the observation of dispersing excitations, which resemble high-frequency sound modes. Liquid alkali metals demonstrated quite clearly propagating acoustic modes over a wide range in wave vectors [37–41]. For more complex liquids, further excitation modes have been proposed, such as the so-called *fast sound* [42], and for charged liquids optic-type modes were predicted by MD simulation and evidenced experimentally [43–45]. For nonionic liquids, only a few experimental studies exist related to optic-type excitations [46–49].

Liquid sulfur might be regarded as a model system to study the fundamental excitations of a molecular-type liquid with the added difficulty that there is a mixture of molecular units. The dynamics of liquid sulfur was investigated by inelastic neutron scattering and inelastic x-ray scattering. In one of the first inelastic neutron scattering experiments, the vibrational density of states was studied with rising temperature [50]. It was reported that the vibrations do not change very much with melting, which was interpreted to indicate that the underlying structure of S_8-rings survives. A further study reported a change in the sharp distinct vibrations during melting [33]. The wave-vector-dependent dynamics was studied with inelastic x-ray scattering, mostly over only a small wave-vector range excluding the main structure factor peak [51,52]. The measurements focused on the low-frequency acoustic-type excitations, and they were analyzed with a simple damped harmonic oscillator model. In a further investigation to elucidate the λ-transition, a viscoelastic reaction of liquid sulfur was assumed in the data analysis [53]. Also Raman spectroscopy was used, and bond-bending vibrations of S_8 rings have been identified in the liquid [54].

Here we present a comprehensive study of the collective dynamics of liquid sulfur. This elemental liquid has the advantage that the analytic difficulties of a molecular liquid with differing scattering properties of the particles are avoided. To reveal details about the collective movements of a molecular-type liquid, the dynamics should be investigated over a wide wave vector and frequency range. To cover a wide range of frequencies and wave vectors, three inelastic neutron scattering experiments have been performed on liquid sulfur. The presented analysis is based on a viscoelastic model with two relaxation times in the memory function. The inclusion of low-frequency relaxation dynamics in the analysis allows a holistic approach in describing the dynamics of this molecular-type liquid. Furthermore, the extension to high frequency measurements opens the door to potential optic-type modes.

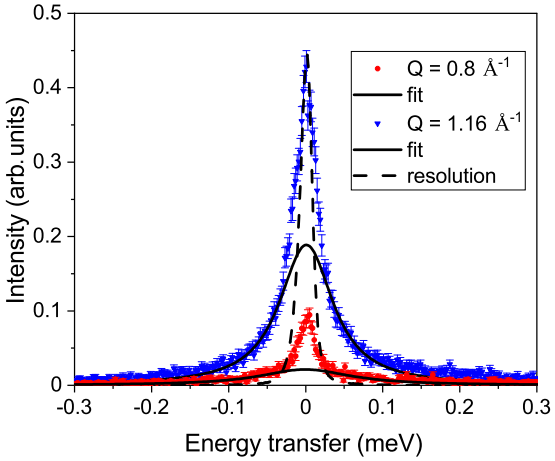

FIG. 1. Two spectra measured with the IRIS spectrometer at $Q = 0.8$ and 1.16 Å^{-1} are plotted together with the peak normalized energy resolution (dashed line). Included as lines are the fit result of the quasielastic contribution.

II. EXPERIMENTAL DETAILS AND DATA ANALYSIS

Three different experiments have been performed to cover a large frequency range. On the indirect tof-backscattering spectrometer IRIS at the ISIS Facility, UK, a high-resolution, low-frequency measurement with PG002 reflection was performed. The final energy was $E_f = 1.84$ meV, with an energy resolution of a full width at half-maximum (FWHM) of 0.018 meV. A small dynamic range ±0.5 meV around the elastic line and Q vectors between 0.5 and 1.8 Å^{-1} were covered. The sulfur sample was kept in a cylindrical aluminum container with a diameter of 22 mm and a wall thickness of 0.5 mm.

For sulfur, the coherent neutron cross section is $\sigma_{\text{coh}} = 1.02$ barn and the incoherent one is negligibly small, $\sigma_{\text{inc}} = 0.008$ barn [55]. In fact, sulfur has one of the smallest neutron cross sections of all elements in the Periodic Table, and hence quite large sample amounts can be used. The sample dimensions correspond to a scattering power of about 6%, and only a small contribution of multiple scattering needs to be considered. Sulfur of 99.998% purity, based on metal trace analysis, was filled into the can. The temperature was controlled by a cryofurnace to $T = 400 \pm 3$ K. In Fig. 1, two spectra at $Q = 0.8$ and 1.16 Å^{-1} are plotted from the IRIS measurement. The intensity of the line increases strongly when the shoulder in the structure factor around $Q = 1.2$ Å^{-1} is approached. Included in one spectrum is the resolution function as a dashed line, measured with a vanadium standard. It clearly demonstrates the relaxation dynamics of liquid sulfur on this frequency range. To reveal the broadening of

the quasielastic line, a fit with a sum of a δ function and a Lorentzian line shape convoluted with the energy resolution was performed. A sloping linear background was added here in the fit model. The Lorentzian contributions from this slow relaxation process are included as lines.

A further experiment was performed with the three-axis spectrometer IN8 at the ILL, Grenoble, France. The spectrometer was operated with a final wave vector $k_f = 3.84$ Å^{-1} corresponding to a final energy $E_f = 30.5$ meV using a Cu200 reflection on the monochromator and a Cu111 reflection on the analyzer. A tight collimation with $30'/20'/20'/30'$ Soller collimators was used. The cryofurnace, holding the sample, was mounted in a 1-m-diam vacuum box to reduce air scattering at small scattering angles. Due to the installed vacuum box and the tight collimation, scattering angles down to 1.5° could be accessed, which is a necessity for observing excitations at small wave vectors. A pyrolytic graphite filter was installed between sample and analyzer to reduce the amount of $\lambda/2$ neutrons. The sulfur sample was the same as for the IRIS experiment, a cylindrical aluminum can with a diameter of 22 mm. The experiment was performed at one temperature $T = 400 \pm 3$ K. The energy resolution, measured with a vanadium standard, in this set up was FWHM = 0.8 meV with a Gaussian line shape. Constant Q-scans from $Q = 0.3$ to 1.9 Å^{-1} were performed with energy transfers ±8 meV in 0.2 meV steps, except at the smallest Q, where the dynamic range was constrained by the kinematics. Up to four runs have been performed for some Q-vectors to increase the statistical quality of the data. For all wave vectors, empty can runs were performed in addition. To cover the high frequency range, the configuration was changed to $E_f = 48$ meV. In this setup with opening up to an open/$60'/60'$/open collimation, the energy resolution increased to FWHM = 4.9 meV with a large increase in neutron flux to detect the weak inelastic signal at large energy transfers. Two wave vectors were scanned at $Q = 1.7$ and 2.0 Å^{-1} over a wide range of energy transfers up to 40 meV with the sulfur sample and the empty can. No second-order filter was used in this configuration, because the amount of higher-order neutrons from the monochromator (larger than 200 meV) is reduced in the Maxwell-Boltzmann distribution of the water moderator.

A third experiment was performed at the three-axis spectrometer IN3 of the ILL, Grenoble, France. That experiment focused on the small-wave-vector region only. A vacuum box was installed on the sample position to reduce the air scattering. As final energy, $E_f = 30$ meV was chosen. Scattering angles down to 1.5° could be measured in a setup with a $40'/40'/60'$ collimation and using a Cu111 monochromator and a PG004 analyzer reflection. The sample was enclosed in an 30-mm-diam aluminum cylinder, which provided 10% scattering power. A transmission measurement confirmed this value in perfect agreement. The heating consisted of heating elements at the bottom and on top of the cell. The temperature was set to $T = 400 \pm 2$ K. Five Q-vectors have been measured, including empty cell runs: $Q = 0.25/0.3/0.35/0.4/0.5$ Å^{-1}. The energy resolution measured with a vanadium standard was FWHM = 1.12 meV. The larger energy resolution caused by a more relaxed collimation and the larger sample diameter are needed due to a much lower flux of the IN3 spectrometer compared to IN8. About

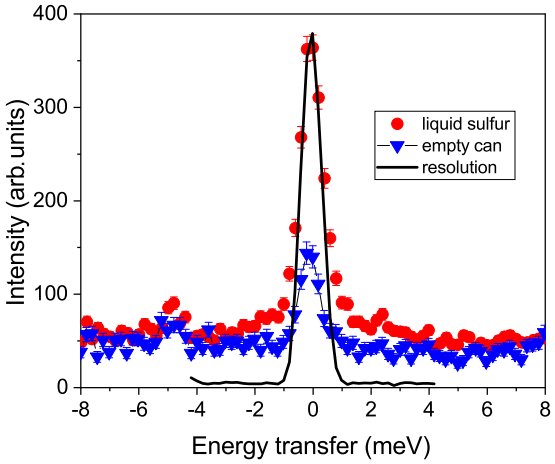

FIG. 2. Raw measured data from the IN8 spectrometer of the sulfur sample at 400 K for $Q = 0.8$ Å^{-1}, the empty can and a peak normalized vanadium scan are plotted.

five scans per Q-vector have been performed. With a typical scan time of 10 min per point, up to 1 h measurement time was therefore used for one scan point. Further measurements keeping the energy transfer at zero and changing the scattering angle to scan $S(Q, \omega \approx \int_{-0.55}^{0.55} d\omega)$ were performed. That measured intensity is related to the structure factor $S(Q)$. Several scans were undertaken during the whole experiment to check for changes in the sample.

The data reduction of the IN8 and IN3 data sets included monitor normalization and an empty can subtraction. In Fig. 2 we plot raw data at $Q = 0.8$ Å^{-1} from the IN8 liquid sulfur measurement and from the empty can. Note that the peak at about −5 meV energy transfer originates from the instrumental background and appears in the sample and empty cell measurement. It can be subtracted properly, as can be seen later in the spectra; see Fig. 7. The line depicts the peak normalized measured resolution from vanadium. An absolute calibration was achieved by comparison with a vanadium standard. The wide energy spectra from the IN8 measurements were symmetrized through multiplication with $\exp(-\hbar\omega/2k_BT)$. With a scattering power of 6% or 10%, the amount of multiple scattered neutrons is consequently quite small. However, the fraction of multiple scattered neutrons into small wave vectors is relatively high compared to other wave-vector ranges. For this reason, a multiple scattering correction for the IN3 and IN8 spectra was performed. The twice scattered signal was computed using as input a viscoelastic model for the single scattering $S(Q, \omega)$ spectrum [41,56]. The obtained twice scattered signal was then intensity-calibrated against the absolute measured signal and subtracted.

To describe the low-frequency excitation spectra, a model function with two components in the memory function was chosen. The Zwanzig-Mori memory function formalism provides a powerful framework to define the dynamics of dense liquids [57,58]. The Laplace transformed relaxation function can be presented in a continued fraction representation:

$$F(Q, z) = \frac{S(Q)}{z + \frac{\omega_0^2}{z + M(Q,z)}}, \tag{1}$$

where ω_0^2 is the normalized second frequency moment of $S(Q,\omega)$, and $M(Q,z)$ is the Laplace transform of the memory function $M(Q,t)$. The dynamic structure factor is related to the real part of $F(Q,z=i\omega)$ through

$$\frac{S(Q,\omega)}{S(Q)} = \frac{1}{\pi}\mathrm{Re}\left[\frac{F(Q,z)}{S(Q)}\right]. \tag{2}$$

A simple approach applies an exponential decaying memory function $M(Q,t) = M(Q,0)\exp(-t/\tau(Q)) = (\omega_l^2 - \omega_0^2)\exp(-t/\tau(Q))$, where the relaxation time $\tau(Q)$ is known as the Maxwell relaxation time. ω_l^2 is the ratio of the fourth to the second frequency moment of the dynamic structure factor [57]. In contrast, the normalized second moment $\omega_0^2 = \frac{k_B T}{mS(Q)}$ is given by the thermal energy and relates to the fluidity of the liquid. The appearance of the structure factor in the denominator reflects the influence of structure on dynamics at larger wave vectors. This single exponential decay in the memory function is the so-called viscoelastic model. An extension of this model adds the contribution from thermal relaxation processes. A specific-heat ratio of $c_p/c_V = 1.14$ [59] for liquid sulfur has been reported, and therefore thermal relaxation processes are not considered relevant for liquid sulfur in contrast to molten salts [45,56]. A straightforward extension of this model consists in adding a further decay process with a scaling factor α in the memory function:

$$M(Q,t) = M(Q,0)[(1-\alpha)\exp(-\Gamma_1(Q)t) + \alpha\exp(-\Gamma_2(Q)t)] \tag{3}$$

with $M(Q,0) = \omega_l^2 - \omega_0^2$. A model with two relaxation times is necessary to describe the complex dynamics of liquid sulfur. A single relaxation time model would not be able to describe the dynamics of collective excitations in the meV range (see Fig. 2) together with the slow relaxation processes shown in the strong quasielastic line; see Fig. 1. The dynamics in this molecular-type liquid covers several decades in frequency and hence needs at least a two-times relaxation model within the memory function.

The Laplace transformed memory function $M(Q,z)$ becomes

$$M(Q,z) = \left(\omega_l^2 - \omega_0^2\right)\left[\frac{(1-\alpha)}{z+\Gamma_1} + \frac{\alpha}{z+\Gamma_2}\right] = \frac{\Delta_1}{z+\Gamma_1} + \frac{\Delta_2}{z+\Gamma_2} \tag{4}$$

with $\Delta_1 = (\omega_l^2 - \omega_0^2)(1-\alpha)$ and $\Delta_2 = (\omega_l^2 - \omega_0^2)\alpha$. Introducing the memory function into the Eq. (1) and then deriving the real part of $F(Q,z)$, an expression for $S(Q,\omega)$ might be obtained; see also [45,56,60]:

$$\frac{S(Q,\omega)}{S(Q)} = \frac{1}{\pi}\frac{\omega^2(f_2 g_3 - f_1 g_4 - f_3 g_2) + f_3 g_4}{\omega^8 + \omega^6\left(f_1^2 - 2g_2\right) + \omega^4\left(g_2^2 + 2g_4 - 2f_1 g_3\right) + \omega^2\left(g_3^2 - 2g_2 g_4\right) + g_4^2}. \tag{5}$$

The f and g parameters are abbreviations for terms involving ω_0^2, ω_l^2, α, $\Gamma_1 = 1/\tau_1$, and $\Gamma_2 = 1/\tau_2$. They are given by $f_1 = \Gamma_1 + \Gamma_2$, $f_2 = \Gamma_1\Gamma_2 + \Delta_1 + \Delta_2$, $f_3 = \Delta_1\Gamma_2 + \Delta_2\Gamma_1$, $g_2 = \Gamma_1\Gamma_2 + \Delta_1 + \Delta_2 + \omega_0^2$, $g_3 = \Delta_1\Gamma_2 + \Delta_2\Gamma_1 + \omega_0^2(\Gamma_1 + \Gamma_2)$, and $g_4 = \omega_0^2\Gamma_1\Gamma_2$.

Figure 3 presents fits with the one-time relaxation model and the two-times relaxation model. Panel (a) shows the $Q = 0.8$ Å data set with the two fits as lines. The two-times model fits the data better and the χ^2 is about a factor 2 smaller. The one-time relaxation model is not capable of describing the slow relaxation process of the strong quasielastic peak together with a rather fast dynamics for the heavily damped excitations. When the fit reduces the least-squares sum around the quasielastic line, the relaxation time becomes too long for a strongly damped inelastic excitation. As a consequence, the fit cannot describe the line shape properly. In contrast, the dynamics of a simple monatomic liquid such as rubidium can be described quite well through a one-time relaxation model, because the quasielastic line amplitude is much more modest compared to the inelastic excitations, which are well expressed and hence not so much damped as in liquid sulfur [41]. The $Q = 0.4$ Å^{-1} data set in panel (b) also shows a better fit with the two-times model, but with a smaller improvement in χ^2. This result evidences that towards a smaller wave vector, a single relaxation time model might be sufficient.

This two-times fit model has six fit parameters—$\omega_l^2(Q)$, $\omega_0^2(Q)$, $\Gamma_1(Q)$, $\Gamma_2(Q)$, $\alpha(Q)$—and an amplitude. To obtain a stable fit over all Q-vectors, the second component of the memory function $\Gamma_2(Q)$, responsible for the slow decay of the quasielastic line, was kept fixed during the fit procedure. The value for this slow decaying part was obtained from the analysis of the high-resolution measurements on IRIS. A fit of the two-times viscoelastic model to IRIS data gave $\Gamma_2 = 0.02$ meV. This value was then used as a fixed parameter for the fit procedure of the IN8 and IN3 spectra, and hence only five fit parameters are used. No background was added in the fit procedure. The reduction of the number of fit parameters resulted in a stable fit procedure that delivered a smooth Q-dependence of the fitted parameters.

In Fig. 4, the measured intensity at the elastic line $S(Q,\omega=0)$ is plotted, obtained through scans at zero energy transfer on the IN3 spectrometer. The intensities are energy-resolution-integrated around the elastic energy, and they illustrate structural changes with temperature. At room temperature, several Debye-Scherrer lines from the polycrystalline structure can be seen. At $T = 400$ K a liquidlike structure appears with a prepeak around $Q \approx 1.2$ Å^{-1} and the main structure factor peak at $Q \approx 1.7$ Å^{-1}. These structural peaks can be understood as the structural pair correlations between the supposed molecular entities in the liquid state [31]. The disorder in the liquid state blurs the well-defined Debye-Scherrer lines from the polycrystalline state.

Several runs at 400 K have been recorded to check for stability of the measurement, and two runs are included in the figure with a few days between them. When the

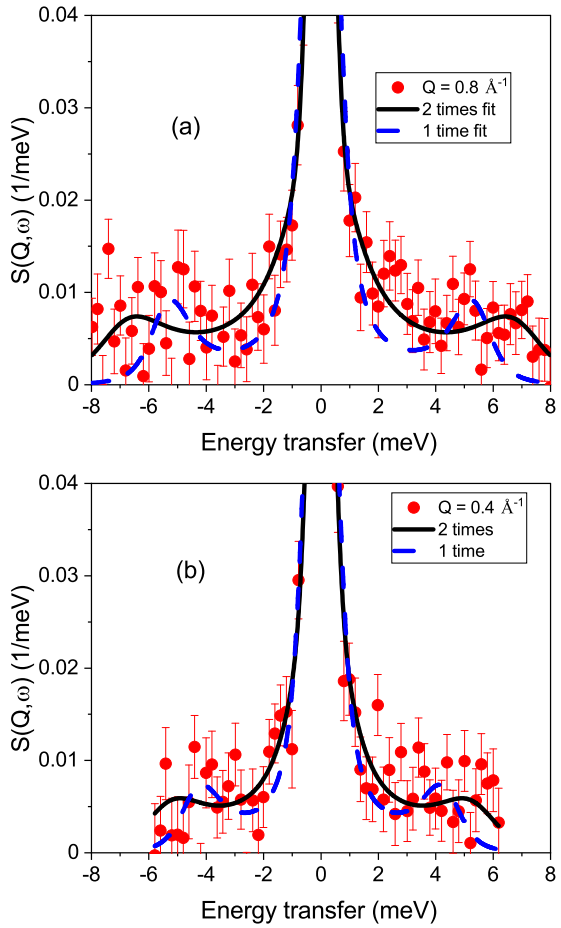

FIG. 3. Panel (a) shows the IN8 data from $Q = 0.8$ Å^{-1} with fits from the single-time and two-times viscoelastic model. In panel (b) the same is plotted for $Q = 0.4$ Å^{-1}.

temperature is raised above the λ-transition (the 530 K run), further characteristic changes appear with a reduction in peak height at the main structure factor position and an increase near the shoulder peak, similar to the reported structural inves-

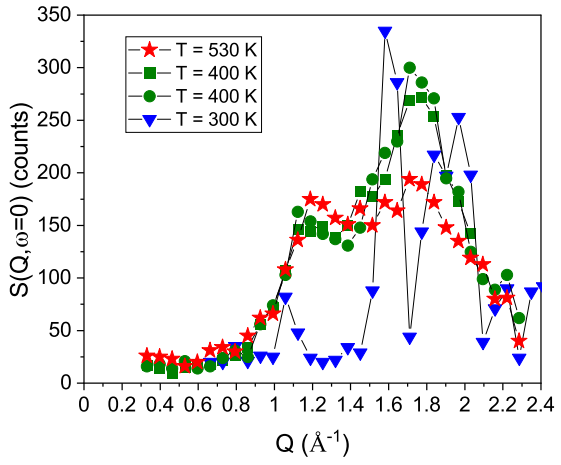

FIG. 4. $S(Q, \omega = 0)$ spectra are shown for different temperatures. The two runs at 400 K have been taken separated by a few days to demonstrate the stability of the measurement.

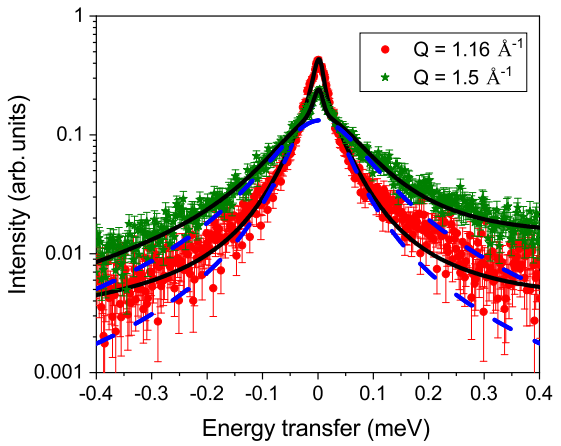

FIG. 5. Two spectra of the high-resolution experiment on IRIS are shown on a logarithmic scale. The solid line depicts the total fit, and the dashed line denotes the quasielastic contribution.

tigations with rising temperature [31]. These measurements confirm that all the spectra have been taken in the liquid state.

III. LOW-FREQUENCY REGION

In Fig. 5, two spectra of liquid sulfur at $Q = 1.16$ and 1.5 Å^{-1} are plotted together with the fit result on a logarithmic scale. Included are the quasielastic component of the fit as a dashed line, which demonstrates the slow relaxation process. The Q-dependence shows that at $Q = 1.16$ Å^{-1} the line shape is sharper and hence the relaxation process slower than at the larger momentum transfer. Relaxation times of around 20–30 ps are quite different from the dynamics to be observed with acoustic-type excitations later on, which are on the sub-ps timescale. This slow relaxation process indicates that a single relaxation process in the memory function will not be sufficient to describe the dynamics over a wide range of frequencies, and hence for a sufficient good modeling of the quasielastic part of the spectrum a further relaxation process needs to be taken into account. There remains still an elastic part in the spectra, which evidences further slow relaxation processes which cannot be resolved with the IRIS spectrometer resolution. Whether this even slower relaxation process might be linked to movements of chainlike structures or whole ring elements needs to be investigated. In Fig. 6, the FWHM of the fit with the Lorentzian line shape and the energy integrated intensity are plotted. A Lorentzian line shape is the simplest approximation for quasielastic relaxations. However, for Q-values around the structure factor maximum, it has been shown that the structural relaxation within the viscoelastic model can be approximated by a Lorentzian line shape with a characteristic relaxation parameter, related to ω_l and ω_0 [57]. Therefore, the Lorentzian line shape used here originates from the viscoelastic model and not from thermal relaxation process as expected for low Q from hydrodynamics. The integrated intensity is a measure for the structure factor $S(Q)$ and shows the expected behavior with a shoulder around $Q \approx 1.2$ Å^{-1} and a further increase towards the main structure peak at about $Q \approx 1.7$ Å^{-1}. The FWHM values agree well with the reported smaller linewidth from an earlier

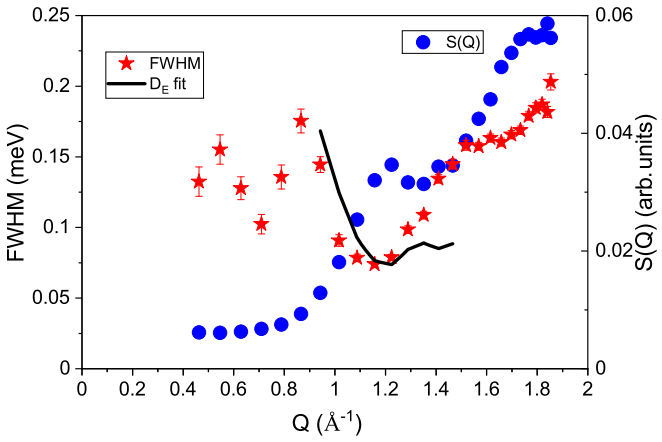

FIG. 6. The FWHMs of the fit with a Lorentzian line shape to the IRIS data are presented. Included is the energy-integrated intensity, which is a measure for the structure factor $S(Q)$. The line depicts the expected Q-dependence of the linewidth according to Eq. (6).

investigation, including the observation of the minimum at $Q \approx 1.2$ Å^{-1} [50]. The second reported larger linewidth is at the limit of our dynamic range and cannot be resolved. The widths show a characteristic dependence with Q with a minimum where the shoulderlike prepeak of the structure occurs at about $Q \approx 1.2$ Å^{-1} and a further minimum is indicated at $Q \approx 1.7$ Å^{-1}. This reduction in linewidth is the signature of the de Gennes narrowing in collective liquid dynamics [61]. In a dense elemental liquid, the particles need time to move to a position that is occupied by another particle, and this increased time is reflected in a reduction of the linewidth. This movement is correlated with movements of other particles that need to create a place for the particle to move. Within kinetic theory for a hard-sphere fluid, the linewidth at the structure factor maximum has been related to a diffusion process, which enables the density fluctuations to decay [62]. Within this formulation, a connection between the Enskog self-diffusion coefficient D_E of a hard-sphere fluid and the measured half-width at half-maximum $\Gamma(Q)$ was established [62]:

$$\Gamma(Q) = \frac{D_E Q^2 d(Q\sigma)}{S(Q)}, \tag{6}$$

where $d(Q\sigma) = [1 - j_0(Q\sigma) + 2j_2(Q\sigma)]^{-1}$ is given by a combination of spherical Bessel functions j_l of order l, and σ denotes the hard-sphere diameter. No Q-limits are known for the validity of Eq. (6) around the minimum, and hence we applied the equation just at the minimum of the linewidth. That relation has successfully been used for elemental and binary liquids [63,64]. The equation strongly resembles the hydrodynamic description of the self-diffusion process, where the structure factor $S(Q)$ takes into account the slowing down of a diffusion process at next-neighbor distances. About 70 years ago, diffusion coefficients from liquid sulfur were reported [17] with a diffusion coefficient of $D = 2.52 \times 10^{-6}$ cm^2/s at $T = 413$ K and $D = 1.52 \times 10^{-6}$ cm^2/s at $T = 399$ K. From the measurement (see Fig. 6) we obtain a HWHM of $\Gamma(Q \approx 1.2$ Å$^{-1}) = 0.037$ meV, and an $S(Q = 1.2$ Å$^{-1}) = 0.7$ has been reported [29,31]. A hard-sphere sulfur diameter of $\sigma = 2.06$ Å can be deduced from the covalent bond length in an S_8 ring. This value agrees with the first peak in the pair correlation function of liquid sulfur [31]. Using these values, we obtain a diffusion coefficient of $D_E = 3.45 \pm 0.06 \times 10^{-6}$ cm^2/s. In Fig. 6 we included the calculated Q-dependent width from Eq. (6) as a line. It demonstrates the correspondence between the structure factor and the width perfectly and also evidences the approximate character concerning the Q-dependence away from the minimum of the linewidth. A diffusion coefficient larger by about 20–30 % can be expected near the melting point, because this hard-sphere approximation only takes binary collisions into account and neglects processes connected to density fluctuations [58,63]. Taking this reduction in diffusion mobility into account, the diffusion coefficient obtained herein agrees reasonably well with the previous macroscopic tracer diffusion measurement. The agreement might be regarded as fortuitous because here a hard-sphere-based theory is applied to a system whose structure factor is only poorly described by a hard-sphere-type model. In addition, a part of the density fluctuation relaxation might stem from a localized rotational motion of the rings and will not contribute to a translational diffusive motion.

IV. THE 1 THz REGIME

Now we will focus on the dynamics with about 1 THz frequency. In Fig. 7 we present several spectra from the measurements with the IN8 spectrometer, and in Fig. 8 spectra from the IN3 instrument are plotted. Included in all the plots are the results from fits with the two-times viscoelastic model. The model describes quite well all measured spectra from both experimental runs.

The spectra are strongly damped, and a distinct excitation is barely visible. The spectral shape is similar to the reported spectra from inelastic x-ray scattering [52]. These strongly damped acoustic modes resemble the excitation spectra of noble gases such as argon [65,66]. The spectra from the collective dynamics of molecular liquids, such as methanol [67], methane [68], or CCl_4 [69], also do not show distinct excitations and resemble the spectra from liquid sulfur. However, the line shape is in contrast to the ones found in liquid alkali metals (see, for example, Refs. [37–41]), where well-defined excitations have been observed over a wide range in wave vectors. Hence the spectra of liquid sulfur are in line with the expected line shape for an insulating liquid.

In Fig. 9 the resulting fit values for ω_l and ω_0 are plotted. The line depicts the adiabatic sound velocity of liquid sulfur at 400 K, which is $c_{ad} = 1350$ m/s. The adiabatic sound velocity agrees well with the fit results for ω_0. The frequencies decrease to zero frequency at small wave vectors, which identifies these excitations as acoustic-type modes. The dispersion of ω_l saturates around 7 meV with weak evidence for a reduction in frequency around $Q \approx 1.7$ Å^{-1}. Overall there is a good agreement between the two different measurements, except maybe at $Q = 0.5$ Å^{-1}. The difference between the two measurements might be related to the different energy resolutions in both experiments. A further reason for the differences might be that over time the amount of ring and chain structures evolve in the melt. Because the IN3 measurements needed up to an order of magnitude longer counting time

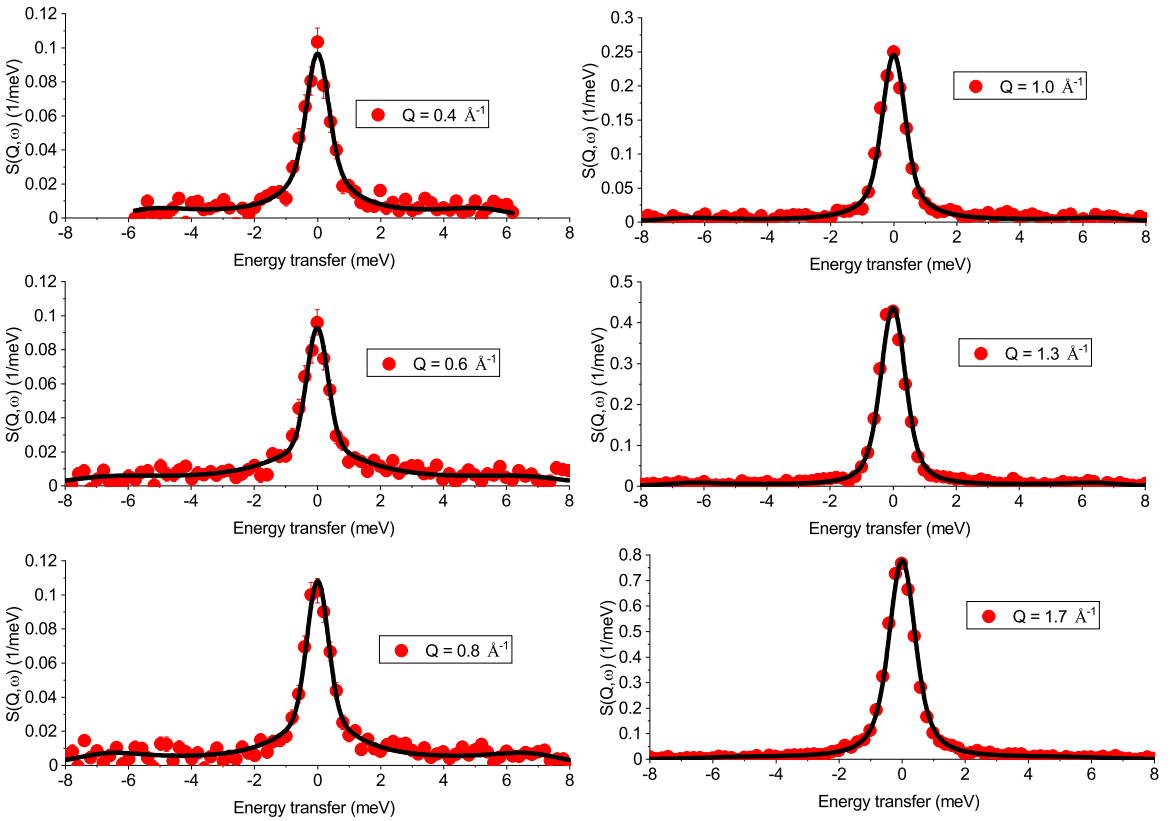

FIG. 7. The plot shows several spectra from the IN8 measurements and included as a line the fit with the two-times viscoelastic model. Note the changing intensity scale for the different wave vectors.

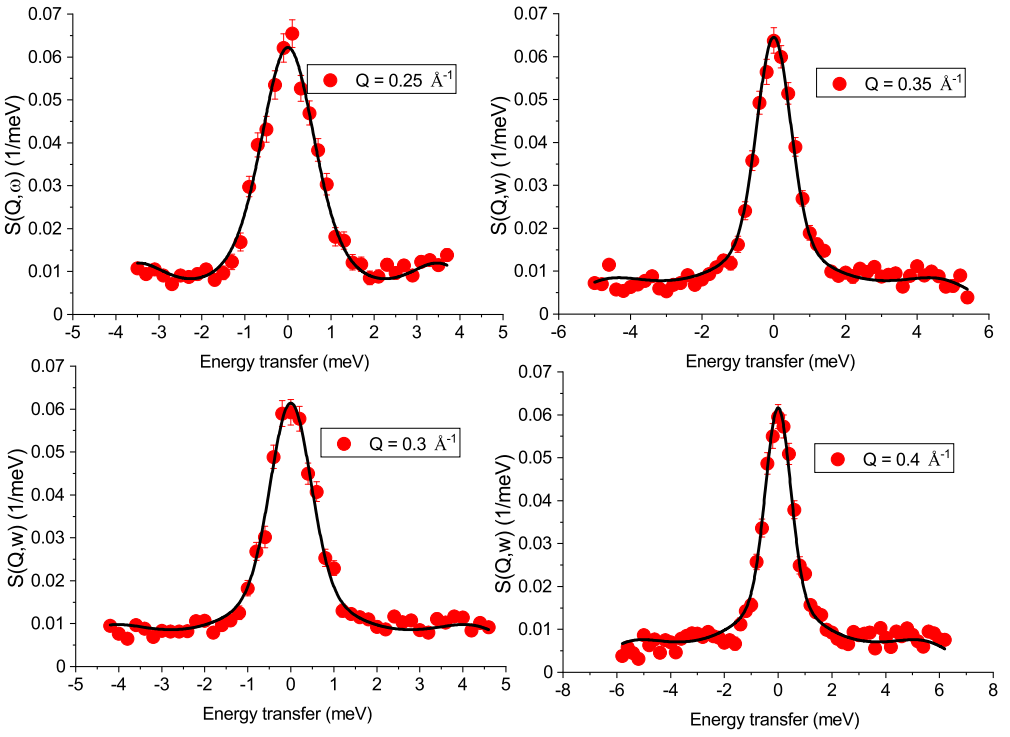

FIG. 8. The plot shows four spectra from the IN3 measurements and included as a line the fit with the two-times viscoelastic model.

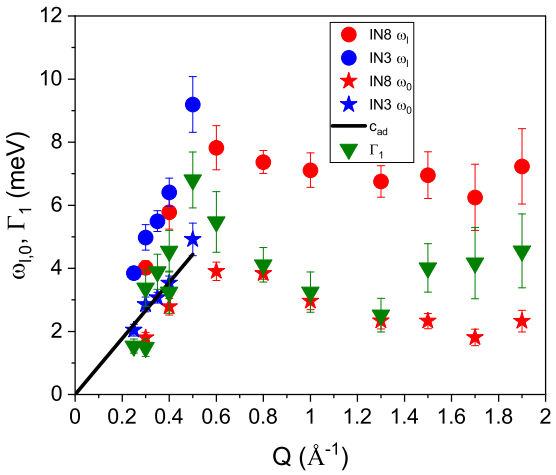

FIG. 9. The results from the fits for ω_l (circles) and ω_0 (stars) are presented from both measurements. The line depicts the adiabatic sound velocity of liquid sulfur. Included are also the fit results for the damping of the memory function Γ_1 (triangles).

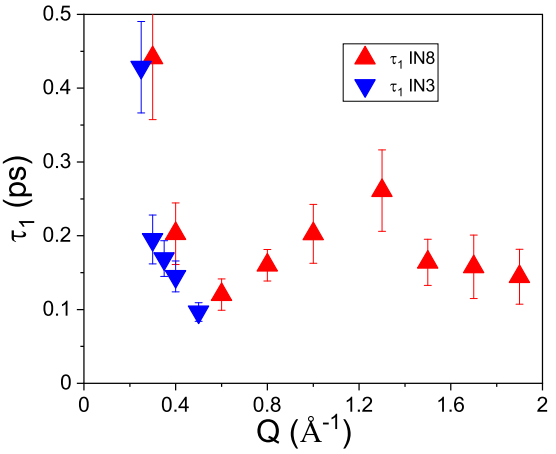

FIG. 10. The relaxation time $\tau_1(Q)$ of the memory function from the fit with the two-times viscoelastic model is plotted against the wave vector for both experiments.

per wave vector due to lower flux on this spectrometer, it might be possible that during the experiment time the exact composition of liquid sulfur has changed. The excitation frequencies are in good agreement with results from inelastic x-ray experiments, even though the energy resolution and data analysis procedures were different [51,52]. The ω_l-values are exceeding the frequency values expected from the adiabatic sound velocity by about 50%. This behavior is called *positive dispersion*, and it has been observed in many liquids. The reason for this increase in sound propagation is the viscoelastic reaction of the liquid towards higher frequencies [57]. When the propagation frequency of the sound excitation exceeds the relaxation rate of the viscous liquid, the liquid reacts solidlike to the density fluctuations and the propagation velocity for sound is shifted to a higher solidlike value. In a previous study, a maximum sound speed of $c = 1870$ m/s was reported [52], whereas we obtain a maximum sound speed of $c = 2200$ m/s. The difference can be understood through the different methods to extract excitation frequencies. For orthorhombic sulfur, phonon dispersion curves have been measured and modeled [70,71]. The range of mode frequencies is very similar to that reported here for the liquid. This agreement supports the idea that a significant number of S_8 rings survive in the liquid state. For liquid Se, a similar enhancement of the sound velocity was reported [72].

The ω_0 values from the IN8 measurement are smaller than the values from the IN3 experiment, and the same applies for Γ_1. This result might be caused by the better energy resolution within the IN8 experiment in combination with a restricted dynamic range in the low-Q region. A dedicated experiment with contradicting requirements such as high energy resolution and wide dynamic range should be performed to resolve this question. Note that the ω_0 values from IN8 in this low-Q range are smaller than the ones expected from the adiabatic sound velocity. Theory predicts that within the viscoelastic model, ω_0 represents the wave-vector generalized sound velocity [57]. The deviation from these expected values could be an indication that the chosen fit model is not capable of describing fully the collective dynamics in liquid sulfur.

Included in Fig. 9 are the relaxation rates $\Gamma_1(Q)$ for both experiments. At small wave vectors Γ_1 increases linearly, and around the shoulder in the structure factor ($Q \approx 1.2$ Å^{-1}) it shows a minimum. We observed a similar behavior with the slow relaxation process; see Fig. 6. For the molecular liquid CCl_4, an enhancement in the sound velocity above the adiabatic value of 37% was reported from inelastic x-ray scattering measurements [69]. The similarity in the line shape and the amount of sound velocity enhancement evidence that the dynamics of liquid sulfur shows elements typical for a molecular liquid.

In Fig. 10 the relaxation time $\tau_1(Q)$ of the memory function is plotted against the wave vector for both experiments. The relaxation times of both experiments agree very well. The values for the fast relaxation times are about a factor 100 smaller than the slow process identified in the high-resolution experiment, which has a relaxation time of about 10–30 ps. Furthermore, this fast relaxation process is influenced by the structure of the liquid. The resulting small $\tau_1(Q)$ values, contrasting the large values from the slow relaxation process, emphasize the wide rate of relaxation processes involved in the liquid sulfur dynamics. In Fig. 11 the contribution α of the second slow relaxation process τ_2 is presented. This slow additional process is needed to describe the small quasielastic linewidth, which hides the slow relaxation dynamics shown in Fig. 1. There is only a small amount needed for this slow process. However, as demonstrated in Fig. 3, without the second relaxation rate in the memory function, no satisfactory line-shape description is possible. Apparently there is a difference in the α value for $Q = 0.3$ Å^{-1} between the IN3 and IN8 measurement, which might be due to different energy resolutions. The reduction in α towards small Q indicates that one relaxation process might be enough in the small-Q regime towards hydrodynamics.

V. THE HIGH-FREQUENCY REGIME

Finally, we are considering the dynamic response at energy transfers beyond 10 meV in liquid sulfur. Two spectra have been obtained in a configuration with a relaxed energy

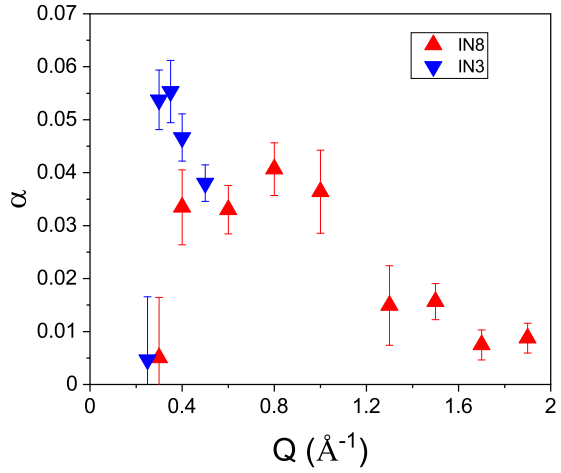

FIG. 11. The contribution of the slow relaxation process α is plotted against the wave vector for both experiments.

resolution to focus on the large energy transfer range. In Fig. 12, spectra at $Q = 1.7$ Å^{-1} (a) and $Q = 2.0$ Å^{-1} (b) are plotted on a logarithmic intensity scale. The spectra demonstrate between 15 and 35 meV a further broad excitation in liquid sulfur. To quantify the excitation, a fit with a damped harmonic oscillator (dho) function has been applied. In the inset, the inelastic part is presented on a linear scale with a fit (line) applying a dho-function [60]. For the mode excitation frequency ω_{dho}, we obtain 28.5 ± 1.4 and 30.0 ± 2.4 meV.

The vibrational density of states has been measured for different states of sulfur [33,50], and some spectra in the fluid state have been recorded [52]. However, no specific inelastic measurements over a wide range of energy transfers and wave-vector resolved exist for liquid sulfur. The vibrational density-of-states measurements identified several bending modes of the S_8 rings from 18 meV up to 30 meV in solid sulfur [33]. After melting, these well-structured modes merge into one broad excitation peak ranging from 18 meV to about 35 meV [33,50]. These frequency values agree with the broad inelastic excitation we observe.

Another dynamic quantity is the current $j(Q, \omega)$. The longitudinal current correlation function is directly linked to the dynamic structure factor through $j(Q, \omega) = \frac{\omega^2}{Q^2} S(Q, \omega)$. Due to the suppression of the quasielastic intensity around zero-energy transfer, inelastic features in the spectra are enhanced. In Fig. 12(c), $j(Q, \omega)$ spectra are plotted, which indicate a further excitation between 20 and 35 meV. The damping of the excitation from the dho-fit is 18 ± 2.4 and 17.6 ± 4 meV and hence it is on the same magnitude as the mode frequency. The strongly damped excitation will oscillate only a few times before dying out.

In a molecular crystal, the force constants between the molecules will determine the acoustic modes. The stronger force constants within the molecules lead to nearly constant frequency optic modes, which represent the internal vibrational modes of the molecule. In solid sulfur, optic modes exist in the range from 18 to 30 meV, which originate from bond-bending modes of the S_8 rings [33]. After melting, a large fraction of ring units survive and the broad excitation between 15 and 35 meV reflects optic-type modes in liquid sulfur. No

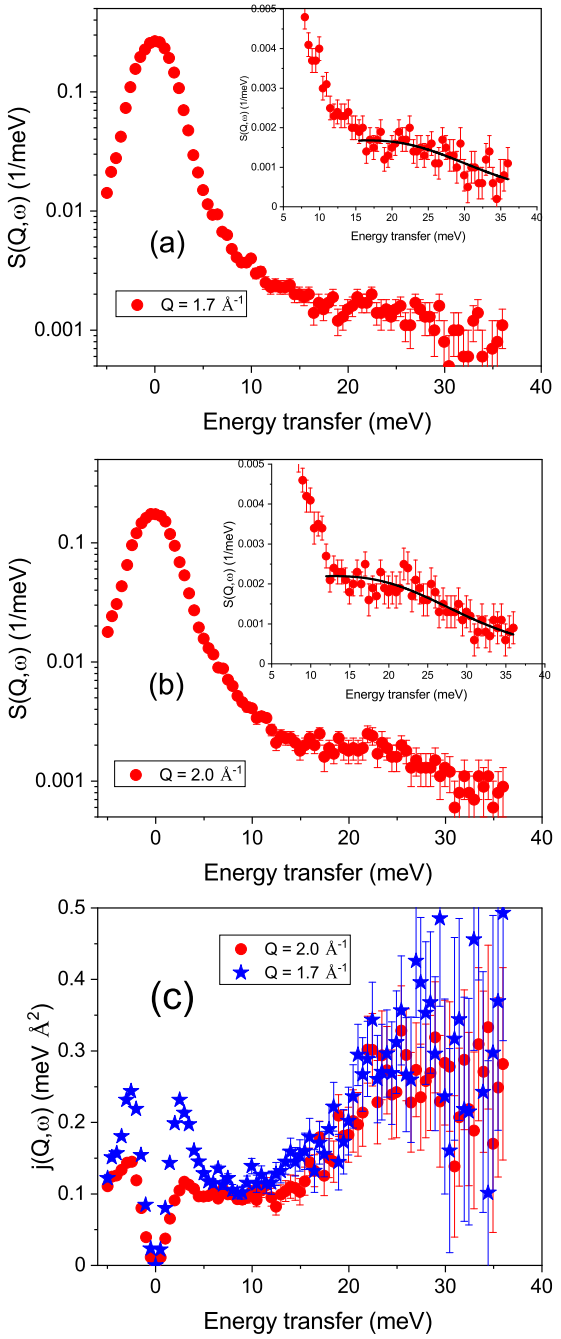

FIG. 12. $S(Q, \omega)$ is plotted for two spectra on a logarithmic scale. The inset shows the high frequency inelastic part on a linear scale including a fit with a dho-model as a line. Panel (c) shows the current correlation functions $j(Q, \omega)$ for $Q = 1.7$ and 2.0 Å^{-1}.

individual excitation mode can be recognized anymore, and the lifetimes of these modes are quite short in the liquid state.

For the next neighbor in this group of the Periodic Table, selenium, more experimental data exist concerning the high-frequency dynamics. Vibrational density-of-states measurements on liquid Se indicated a broad peak around the region where bond-bending modes are expected [73]. From inelastic neutron scattering experiment on liquid Se, it was concluded that the high-frequency excitation around 31 meV has an optic-type character [46,74]. These statements agree

with our conclusion that we observe optic-type modes in liquid sulfur.

VI. CONCLUSIONS

We performed three inelastic neutron scattering experiments on liquid sulfur above the melting point and below the transition to a high-viscous polymerized state. The three experiments covered three decades in relaxation and excitation dynamics and revealed collective dynamics from about 30 μeV to 30 meV in energy. The wide range of frequencies can be traced back to the nonsimple structure of this elemental liquid. A slow relaxation process with a relaxation rate of about 10 GHz was identified in a high-resolution experiment. It showed a wave-vector dependence typical for de Gennes narrowing. Identifying this relaxation process with a diffusion step, a diffusion coefficient could be obtained, which agrees reasonably well with a result from macroscopic tracer diffusion measurements. A further localized rotational movement of the eight-membered sulfur rings might be hidden in this signal. Evidence exists that even slower movements occur in liquid sulfur.

The low-frequency excitations in the 1 THz regime can be described as strongly damped acoustic modes. Their description needs a viscoelastic model with two relaxation processes in the memory function. The two timescales are separated by two orders of magnitude, where the slow one is near the relaxation process identified in the high-resolution experiment. The fast and dominating process is responsible for the damping of the acoustic modes. The spectral line shape and the enhancement of the sound velocity is in accord with reports from typical molecular liquids and evidences that liquid sulfur can be regarded as a molecular liquid.

At high frequency, around 10 THz, a broad mode was identified, which lies where the crystal shows several distinct optic modes. We interpret this excitation as the reminiscence of optic modes in the liquid. In summary, a quite broad and detailed description was presented for the collective dynamics of liquid sulfur, which could instigate more detailed studies from scattering experiments and MD-simulation. In particular, the nature of even slower relaxation processes needs clarification. With the presented results, the foundations are there for an approach to study the changes with crossing the polymerization transition in detail. Our study might also provide some insight into the collective dynamics of a wide range of molecular liquids.

ACKNOWLEDGMENTS

We acknowledge support from the Science and Technology Facilities Council, STFC. The sample environment groups at the facilities are thanked for their support. The continuous encouragement from J. L. Hazemann during several phases of the project is highly appreciated.

[1] B. Meyer, Chem. Rev. **76**, 367 (1976).
[2] R. Steudel and B. Eckert, Top. Curr. Chem. **230**, 1 (2003).
[3] S. J. Rettig and J. Trotter, Acta Crystallogr., Sect. C **43**, 2260 (1987).
[4] R. F. Bacon and R. Fanelli, J. Am. Chem. Soc. **65**, 639 (1943)
[5] J. Ruiz-Garcia, E. M. Anderson, and S. C. Greer, J. Phys. Chem. **93**, 6980 (1989).
[6] G. E. Sauer and L. B. Borst, Science **158**, 1567 (1967).
[7] A. V. Tobolsky and A. Eisenberg, J. Am. Chem. Soc. **81**, 780 (1959).
[8] A. V. Tobolsky and A. Eisenberg, J. Am. Chem. Soc. **82**, 289 (1960).
[9] A. Eisenberg and L. A. Teter, J. Phys. Chem. **71**, 2332 (1967).
[10] H. Patel and L. B. Borst, J. Chem. Phys. **54**, 822 (1971).
[11] A. Eisenberg, Macromolecules **2**, 44 (1969).
[12] V. F. Kozhevnikov, J. M. Viner, and P. C. Taylor, Phys. Rev. B **64**, 214109 (2001).
[13] M. J. Stashick and R. A. Marriott, J. Chem. Phys. **152**, 044503 (2020).
[14] A. D. Alvarenga, M. Grimsditch, S. Susman, and S. C. Rowland, J. Phys. Chem. **100**, 11456 (1996).
[15] B. Yuan, B. Aitken, and S. Sen, J. Chem. Phys. **151**, 041105 (2019).
[16] K. S. Andrikopoulos, A. G. Kalampounias, and S. N. Yannopoulos, J. Chem. Phys. **124**, 146101 (2006).
[17] R. L. Saxton and H. G. Drickamer, J. Chem. Phys. **21**, 1362 (1953).
[18] S. Hosokawa, T. Masuoka, and K. Tamura, J. Phys.: Condens. Matter **6**, 5273 (1994).
[19] E. D. West, J. Am. Chem. Soc. **81**, 29 (1959).
[20] L. Crapanzano, W. S. Crichton, G. Monaco, R. Bellisent, and M. Mezouar, Nat. Mater. **4**, 550 (2005).
[21] L. Henry, M. Mezouar, G. Garbarino, D. Sifre, G. Weck, and F. Datchi, Nature (London) **584**, 382 (2020).
[22] G. O. Sofekun, E. Evoy, K. L. Lesage, N. Chou, and R. A. Marriott, J. Rheol. **62**, 469 (2018).
[23] D. Alfe and M. J. Gillan, Phys. Rev. B **58**, 8248 (1998).
[24] G. Zhou, A. Yang, G. Gao, X. Yu, J. Xu, C. Liu, Y. Ye, A. Pei, Y. Wu, Y. Peng, Y. Li, Z. Liang, K. Liu, L.-W. Wang, and Y. Cui, Sci. Adv. **6**, eaay5098 (2020).
[25] R. Winter, T. Bodensteiner, C. Szornel, and P. A. Egelstaff, J. Non-Cryst. Solids **106**, 100 (1988).
[26] R. Bellissent, L. Descotes, F. Boue, and P. Pfeuty, Phys. Rev. B **41**, 2135 (1990).
[27] C. W. Tompson and N. S. Gingrich, J. Chem. Phys. **31**, 1598 (1959).
[28] K. S. Vahvaselkä and J. M. Mangs, Phys. Scr. **38**, 737 (1988).
[29] M. Stolz, R. Winter, W. S. Howells, R. L. McGreevy, and P. A. Egelstaff, J. Phys.: Condens. Matter **6**, 3619 (1994).
[30] R. Bellissent, L. Descotes, and P. Pfeuty, J. Phys.: Condens. Matter **6**, A211 (1994).
[31] R. Winter, C. Szornel, W. C. Pilgrim, W. S. Howells, P. A. Egelstaff, and T. Bodensteiner, J. Phys.: Condens. Matter **2**, 8427 (1990).
[32] R. Winter, P. A. Egelstaff, W. C. Pilgrim, and W. S. Howells, J. Phys.: Condens. Matter **2**, SA215 (1990).
[33] Chr. Biermann, R. Winter, Chr. Benmore, and P. A. Egelstaff, J. Non-Cryst. Solids **232**, 309 (1998).

[34] F. H. Stillinger, T. A. Weber, and R. A. LaViolette, J. Chem. Phys. **85**, 6460 (1986).
[35] J. S. Tse and D. D. Klug, Phys. Rev. B **59**, 34 (1999).
[36] D. Plašienka, P. Cifra, and R. Martonak, J. Chem. Phys. **142**, 154502 (2015).
[37] J. R. D. Copley and J. M. Rowe, Phys. Rev. Lett. **32**, 49 (1974).
[38] T. Bodensteiner, Chr. Morkel, W. Gläser, and B. Dorner, Phys. Rev. A **45**, 5709 (1992).
[39] H. Sinn, F. Sette, U. Bergmann, C. Halcoussis, M. Krisch, R. Verbeni, and E. Burkel, Phys. Rev. Lett. **78**, 1715 (1997).
[40] W.-C. Pilgrim, S. Hosokawa, H. Saggau, H. Sinn, and E. Burkel, J. Non-Cryst. Solids **250-252**, 96 (1999).
[41] F. Demmel, D. Pasqualini, and C. Morkel, Phys. Rev. B **74**, 184207 (2006).
[42] J. Bosse, G. Jacucci, M. Ronchetti, and W. Schirmacher, Phys. Rev. Lett. **57**, 3277 (1986).
[43] F. Demmel, S. Hosokawa, W.-C. Pilgrim, and S. Tsutsui, Nucl. Instrum. Methods Phys. Res., Sect. B **238**, 98 (2005).
[44] S. Hosokawa, M. Inui, T. Bryk, I. Mryglod, W.-C. Pilgrim, Y. Kajihara, K. Matsuda, Y. Ohmasa, and S. Tsutsui, Condens. Matter Phys. **22**, 43602 (2019).
[45] F. Demmel, S. Hosokawa, and W.-C. Pilgrim, J. Phys.: Condens. Matter **33**, 375103 (2021).
[46] A. Chiba, Y. Ohmasa, M. Yao, and S. M. Bennington, J. Neutron Res. **12**, 301 (2004).
[47] L. E. Bove, F. Formisano, E. Guarini, A. Ivanov, C. Petrillo, and F. Sacchetti, Europhys. Lett. **79**, 16002 (2007).
[48] F. Demmel, G. Heusel, I. Waldner, J. Stride, and H. Bertagnolli, Z. Phys. Chem. **222**, 1551 (2008); F. J. Bermejo, J. W. Taylor, S. E. McLain, I. Bustinduy, J. F. C. Turner, M. D. Ruiz-Martin, C. Cabrillo, and R. Fernandez-Perea, Phys. Rev. Lett. **96**, 235501 (2006).
[49] S. Jahn and J. B. Suck, Phys. Rev. Lett. **92**, 185507 (2004).
[50] L. Descôtes, R. Bellisent, P. Pfeuty, and A. J. Dianoux, Physica A **201**, 381 (1993).
[51] G. Monaco, L. Crapanzano, R. Bellissent, W. Crichton, D. Fioretto, M. Mezouar, F. Scarponi, and R. Verbeni, Phys. Rev. Lett. **95**, 255502 (2005).
[52] M. Inui, Y. Kajihara, A. Chiba, K. Matsuda, S. Tsutsui, and A. Q. R. Baron, J. Non-Cryst. Solids **522**, 119571 (2019).
[53] T. Scopigno, S. N. Yannopoulos, F. Scarponi, K. S. Andrikopoulos, D. Fioretto, and G. Ruocco, Phys. Rev. Lett. **99**, 025701 (2007).
[54] K. Hattori and H. Kawamura, J. Non-Cryst. Solids **59**, 1063 (1983).
[55] V. F. Sears, Neutron News **3**, 26 (1992).
[56] F. Demmel, D. Szubrin, W. C. Pilgrim, A. De Francesco, and F. Formisano, Phys. Rev. E **92**, 012307 (2015).
[57] U. Balucani and M. Zoppi, *Dynamics of the Liquid State* (Clarendon, Oxford, 1994).
[58] J. P. Hansen and I. McDonald, *Theory of Simple Liquids* (Academic, London, 2006).
[59] O. J. Kleppa, J. Chem. Phys. **18**, 1303 (1950).
[60] U. Bafile, E. Guarini, and F. Barocchi, Phys. Rev. E **73**, 061203 (2006).
[61] P. G. De Gennes, Physica **25**, 825 (1959).
[62] E. G. D. Cohen, P. Westerhuijs, and I. M. de Schepper, Phys. Rev. Lett. **59**, 2872 (1987).
[63] F. Demmel, D. Szubrin, W.-C. Pilgrim, and C. Morkel, Phys. Rev. B **84**, 014307 (2011).
[64] F. Demmel, O. Alcaraz, and J. Trullas, Phys. Rev. E **93**, 042604 (2016).
[65] K. Sköld, J. M. Rowe, G. Ostrowski, and P. D. Randolph, Phys. Rev. A **6**, 1107 (1972).
[66] A. A. van Well, P. Verkerk, L. A. de Graaf, J. B. Suck, and J. R. D. Copley, Phys. Rev. A **31**, 3391 (1985).
[67] F. J. Bermejo, F. Batallan, J. L. Martinez, M. Garcia-Hernandez, and E. Enciso, J. Phys.: Condens. Matter **2**, 6659 (1990).
[68] E. Guarini, U. Bafile, F. Barocchi, F. Demmel, F. Formisano, M. Samploi, and G. Venturi, Europhys. Lett. **72**, 969 (2005).
[69] T. Kamiyama, S. Hosokawa, A. Q. R. Baron, S. Tsutsui, K. Yoshida, W. C. Pilgrim, Y. Kiyanagi, and T. Yamaguchi, J. Phys. Soc. Jpn. **73**, 1615 (2004).
[70] R. P. Rinaldi and G. S. Pawley, J. Phys. C **8**, 599 (1975).
[71] T. Luty and G. S. Pawley, Phys. Status Solidi B **69**, 551 (1975).
[72] M. Inui, S. Hosokawa, K. Matsuda, S. Tsutsui, and A. Q. R. Baron, Phys. Rev. B **77**, 224201 (2008).
[73] W. Phillips, U. Buchenau, N. Nücker, A. J. Dianoux, and W. Petry, Phys. Rev. Lett. **63**, 2381 (1989).
[74] A. Chiba, Y. Ohmasa, S. M. Bennington, J. W. Taylor, and M. Yao, Phys. Rev. B **77**, 132202 (2008).